

## Article

# Similariton-like Pulse Evolution in an Er-Doped Fiber Laser with Hybrid Mode Locking

Aleksander Y. Fedorenko , Almikdad Ismaeel, Ilya O. Orekhov, Dmitriy A. Dvoretzkiy ,  
Stanislav G. Sazonkin , Lev K. Denisov and Valeriy E. Karasik

Research and Education Center “Photonics and IR-Techniques”, Bauman Moscow State Technical University, 105005 Moscow, Russia; ismailal@bmstu.ru (A.I.); orekhovio@bmstu.ru (I.O.O.); ddvoretzkiy@bmstu.ru (D.A.D.); sazstas@bmstu.ru (S.G.S.); l.denisov@bmstu.ru (L.K.D.); karassik@bmstu.ru (V.E.K.)

\* Correspondence: fedorenko@bmstu.ru

**Abstract:** An Er-doped all-fiber ultrashort pulse laser with positive total net-cavity group-velocity dispersion is demonstrated based on a hybrid mode-locking mechanism ensured by single-walled carbon–boron–nitrogen nanotubes with coaction of the nonlinear polarization evolution effect. The generation regime with a similariton-like spectrum is obtained. The spectrum width is ~31.5 nm, and the minimal pulse duration is ~294 fs at full width at half maximum. The average output power is ~3.2 mW, corresponding to 0.376 nJ pulse energy and 1.25 kW peak power. The fundamental pulse repetition rate is ~8.5 MHz, with a signal-to-noise ratio of 60 dB. The standard deviation of average output optical power stability, measured for 12 h, is about ~1% RMS, and the maximum level of relative intensity noise (RIN) does not exceed  $< -120$  dBc/Hz in the 30 Hz–1 MHz frequency range. To prove the similariton-like regime generation, we also studied numerically and experimentally the pulse evolution during propagation through a laser resonator and output single-mode fiber with anomalous dispersion.

**Keywords:** similariton-like pulses; erbium-doped fiber lasers; ultrashort pulse generation; pulse evolution



**Citation:** Fedorenko, A.Y.; Ismaeel, A.; Orekhov, I.O.; Dvoretzkiy, D.A.; Sazonkin, S.G.; Denisov, L.K.; Karasik, V.E. Similariton-like Pulse Evolution in an Er-Doped Fiber Laser with Hybrid Mode Locking. *Photonics* **2024**, *11*, 387. <https://doi.org/10.3390/photonics11040387>

Received: 3 April 2024  
Revised: 18 April 2024  
Accepted: 19 April 2024  
Published: 21 April 2024



**Copyright:** © 2024 by the authors. Licensee MDPI, Basel, Switzerland. This article is an open access article distributed under the terms and conditions of the Creative Commons Attribution (CC BY) license (<https://creativecommons.org/licenses/by/4.0/>).

## 1. Introduction

Ultrashort pulse (USP) lasers with high short-term stability of amplitude and frequency parameters are of great importance in such high-precision areas as frequency comb spectroscopy [1,2], optical frequency standards [3,4] and microwave signal generation [5–7]. In recent years, much attention has been paid to the study of various methods for short-term stabilization of USP radiation and the development of mode-locked sources with low noise performance [8–10].

The active short-term stabilization method based on an active electronic feedback loop is widely used for the suppression of intensity noise in mode-locked lasers. It usually includes a pump current modulator for compensation of laser diode intensity fluctuations [11] and a transmittance control system for the acousto-optic modulator [12]. Although this method allows the achievement of relative intensity noise (RIN) levels below  $-140$  dBc/Hz at a radio frequency of 100 Hz [11,13], it has a significant disadvantage: in the region of the feedback control band, there is a strong resonant peak, and, as a result, the integrated noise intensity increases.

At present, the control of total intracavity group velocity dispersion (GVD) toward the near-zero region is one of the most common passive methods for the suppression of intensity noise and timing jitter [10,14]. As is known, in the region of zero GVD, there are two main generation regimes that may be observed: stretched pulses [15] and similaritons [16]. The key property that distinguishes a similariton regime from a stretched pulse regime is the absence of significant pulse energy limitations caused by dispersive waves formation, and, as a result, similaritons have the potential to create high-power laser systems [17,18].

Similaritons are pulses described by asymptotic self-similar solutions of the modified nonlinear Schrödinger equation (NLSE) with positive linear chirp [16]. This generation regime has a parabolic pulse shape and a parabolic spectrum and is realized at a positive total net-cavity GVD. The passive similaritons [16] considered in this study, in contrast to amplifier similaritons [19], are formed in dispersion-managed cavities and with minimal spectral filtering. Such pulses remain self-similar even in the passive fiber and do not act as a nonlinear attractor. Similaritons are stable as long as the envelope of the optical spectrum does not expand beyond the amplification band of the active medium [17].

Another straightforward approach to passive noise suppression is the use of bandpass filters that reduce both RIN [13] and timing jitter [19]. However, it should be noted that spectral filtering inevitably leads to an increase in pulse duration [20] and insertion loss.

One of the promising methods for short-term stabilization of mode-locked fiber lasers may be the use of hybrid mode locking in resonators, a combination of natural and artificial saturable absorbers (SAs). Most USP lasers operate with passive mode locking, using two types of SAs: natural SAs—semiconductor saturable absorber mirrors (SESAMs), single-walled nanotubes and graphene; and artificial SAs—the mechanism of nonlinear evolution of polarization (NPE), the principles of nonlinear optical loop mirror (NOLM) and nonlinear amplifying loop mirrors (NALMs) [21–26]. Both types of SAs have their advantages and disadvantages, and their combination allows one to mutually compensate for the other, and, as a result, it is possible to achieve higher time and frequency stability [27–29].

When developing lasers with the use of the methods discussed above, one of the key problems is the difficulty of assessing the direct influence of the applied technical solutions on each other and on the parameters of the generated pulses. This problem is especially acute for lasers with positive intracavity GVD due to the more complex dynamics of pulse formation and propagation. Most studies researching the dynamics of the formation and evolution of pulses in USP lasers with a positive net-cavity dispersion are devoted to searching for the energy limitations of the generation regimes existence [18,30–32]. However, many investigations have been reported on the dynamics of pulse generation inside a laser cavity. For example, Chong et al. [33] performed mathematical modelling of a Yb-doped fiber laser operating in all-normal dispersion (ANDi) with SA in the form of NPE and demonstrated the formation of self-similar and M-shaped dissipative soliton pulses, noting the key role of the spectral filter in this process. Boscolo with colleagues [32] reported a numerical study of similariton dynamics inside the cavity of a Yb-doped fiber laser operating at anomalous net-cavity GVD. Luo et al. [34] conducted experimental research on the pulse evolution inside the cavity of an Er-doped fiber laser with large positive dispersion, where four output couplers were added to the cavity. To study the evolution of radiation, the dispersive Fourier transform (DFT) technique is also used [31], which allows one to study the dynamics depending on the number of pulse round trips through the resonator.

In this paper, we demonstrate both numerical and experimental studies of the similariton evolution in an Er-doped fiber laser with hybrid mode locking. In order to carry out such an investigation, we used an SMF-28 fiber stretcher–compressor at the resonator output, which is equivalent to the SMF-28 section inside the resonator, adjusted for the fact that radiation with four times less power propagates through it, and changed its length. The experimental data were compared with the numerical model. As a result, the characteristics of the spectrum and pulse duration at the minimum and maximum lengths were almost equivalent, with a more pronounced spectral filtering effect as the output fiber length increased.

## 2. Materials and Methods

The experimental setup for the all-fiber erbium-doped laser resonator is shown in Figure 1. The resonator is formed with fiber of 3 types, which makes it possible to implement the net-cavity dispersion control mechanism. First is Erbium-doped fiber HE980 (Lucent Technologies Inc., Murray Hill, NJ, USA) with a core absorption of ~4 dB/m and a

dispersion parameter of  $D \sim -54.6 \text{ ps}/(\text{nm}\cdot\text{km})$ , which serves as an active laser medium. In order to increase the pump absorption efficiency, 6.09 m of this fiber is used in the resonator. The second type of fiber is the passive SMF-28 fiber (Corning Inc., New York, NY, USA) with a dispersion parameter of  $D \sim +17.4 \text{ ps}/(\text{nm}\cdot\text{km})$  and a length of 18.21 m. In order to achieve the overall intracavity GVD required for the parabolic pulse generation, the main adjustment of the dispersion is realized by changing the SMF-28 length. The third fiber type is CS980, with a dispersion parameter of  $D \sim -2.16 \text{ ps}/(\text{nm}\cdot\text{km})$  [35] and a length of 2.045 m, and it is used to connect WDM 980/1550 to EDF. All dispersion coefficients are given at a wavelength of 1550 nm. The total length of the resonator is 26.5 m, and the total net-cavity dispersion is slightly positive ( $\beta_2 = +0.025 \text{ ps}^2$  at 1530 nm). A CW laser diode (LC96A74P-20R, Oclaro Inc., San Jose, CA, USA) operating at a wavelength of 980 nm is used as the pump source. To input and output the pump radiation, two wave demultiplexing filters (WDM 980/1550) are used. As a result of the property of spectral selectivity, they also play the role of a spectral filter, preventing expansion of the optical spectrum. The polarization-maintaining fiber isolator (ISO-PM) is used to ensure unidirectional generation. A fiber coupler is also used to extract lasing radiation from the resonator: 80% of the radiation remains in the resonator, and 20% is removed.

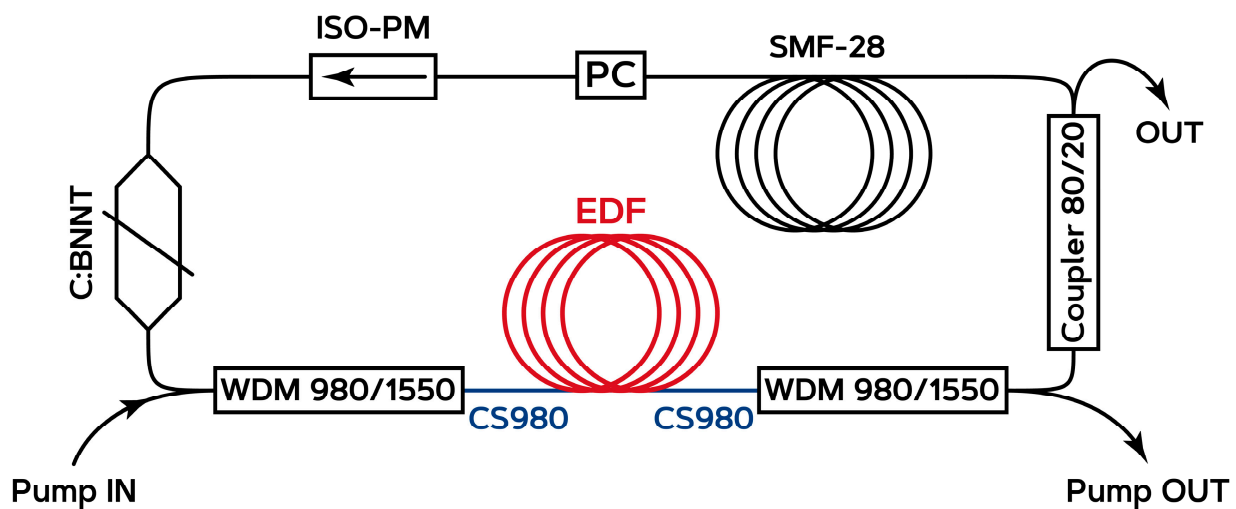


**Figure 1.** The experimental setup of the Erbium-doped all-fiber USP laser with a hybrid mode-locking mechanism.

The resonator operates with the hybrid mode locking (ML) regime using both fast and slow saturable absorbers. Single-walled carbon–boron–nitride nanotubes (C:BNNTs) act as slow saturable absorbers, enabling the launch of the ML regime. Such materials provide a relatively low mode-locking threshold and a shorter pulse generation compared to common carbon nanotubes [36]. The role of a fast saturable absorber is played by the NPE effect [29]. To control ML, a polarization controller (PC) is installed in the cavity.

### 3. Experimental Results

Slightly positive net-cavity GVD pulses, formed in the ML fiber laser cavity, can tend to have a parabolic shape. The spectrum of our generation regime, shown in Figure 2a, is well approximated by the parabolic function in contrast to the Gaussian form, which may indicate that the regime we are studying is similariton-like.

The data shown in Figure 2 were taken at a fiber compressor length of  $\sim 5.1 \text{ m}$ , at which the minimum pulse duration was reached. The optical spectrum of a similariton-like pulse experimentally measured using the CMA5000a optical spectrum analyzer (Anritsu Corporation, Atsugi, Japan) had a central wavelength at 1530 nm and a full width at half maximum (FWHM) of  $\sim 31.5 \text{ nm}$ .

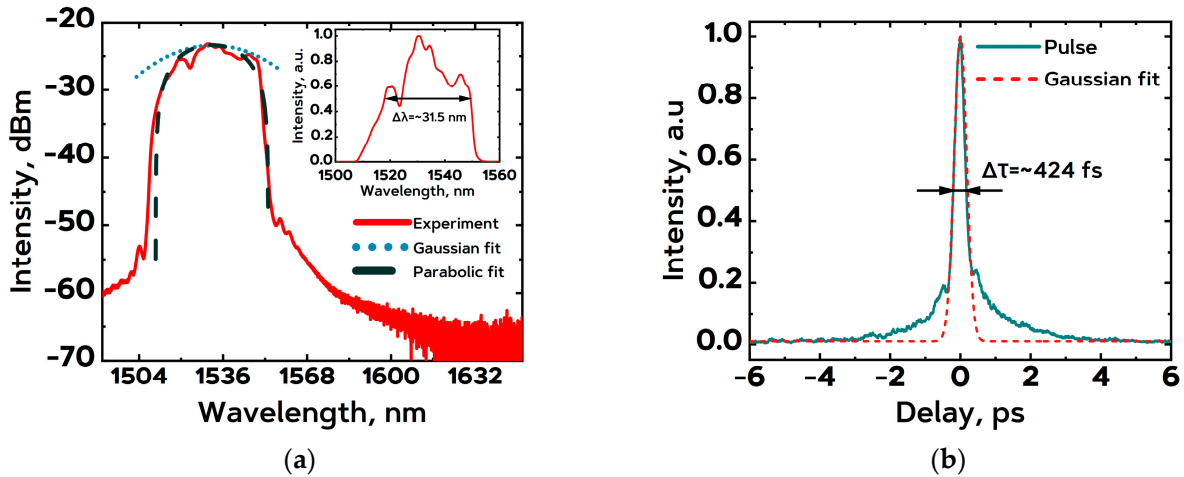


**Figure 2.** (a) Optical spectrum of output radiation, approximated with Gaussian and parabolic functions, and spectrum of the radiation in relative units (inset). (b) Intensity autocorrelation trace with Gaussian fitting and pulse intensity temporal profile with phase (inset).

To estimate the USP duration, the intensity autocorrelation trace was measured after 15 rounds of averaging, as shown in Figure 2b (performed with the FR-103 WS autocorrelator (FEMTOCHROME RESEARCH Inc., Berkeley, CA, USA)). This graph indicates an intensity autocorrelation width with a Gaussian approximation of  $\sim 424$  fs at FWHM that corresponds to the duration of the pulse equal to  $\sim 424 \times 0.707 = \sim 294$  fs.

It is important to note that sometimes the optical spectrum shape and net-cavity GVD are not sufficient for generation regime identification, especially in the zero-dispersion region. To ensure accurate categorization, we measured the pulse intensity temporal profile and phase (using GRENOUILLE 15–40 USB (Swamp Optics LLC, Atlanta, GA, USA)), as shown in Figure 3. The pulse FWHM, as determined by the temporal profile (Figure 3b), is 272 fs. It closely matches the measurement obtained from the autocorrelation trace, confirming its representativeness.

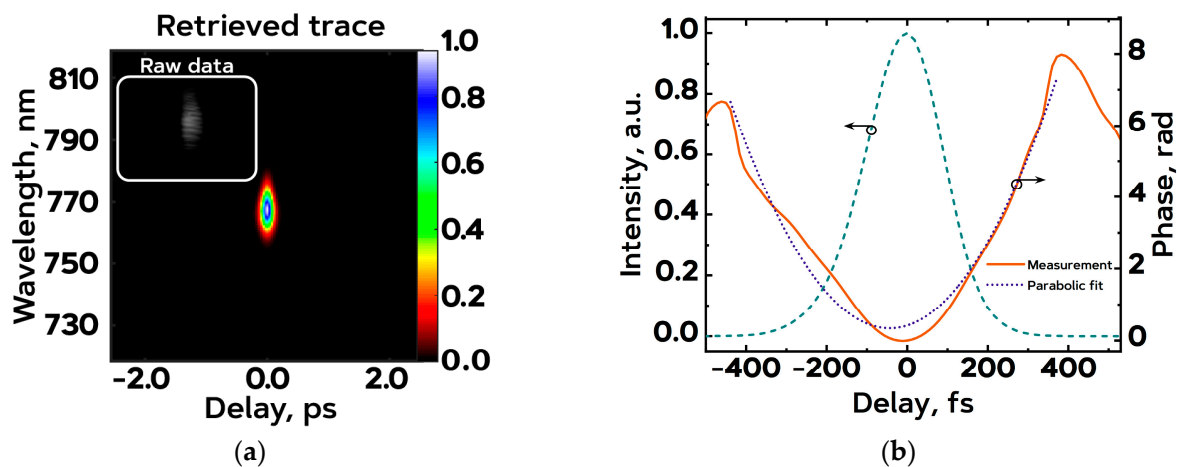


**Figure 3.** (a) Retrieved GRENOUILLE trace with raw data (inset). (b) Pulse temporal intensity profile (blue) and measured phase (orange) with parabolic fit (purple).

A slightly more detailed consideration of the phase is necessary. As mentioned in the introduction, the similariton generation regime is distinguished by a linear positive chirp, meaning that the instantaneous frequency is a linear and increasing function. As a reminder, the phase is the integral of the instantaneous frequency over time. Consequently, it should have the form of a parabolic function with upward branches for similariton pulses [37]. The measured phase corresponds exactly to the case considered above. Therefore, we

can unambiguously state that the generation regime under study is similariton-like. The maximum average output optical power was  $\sim 3.2$  mW at a 450 mW pump power; this means that the pulse energy was about 0.376 nJ and that the peak power was 1.25 kW. A further increase in the peak power may be achieved by using an erbium-doped fiber amplifier (EDFA) after the laser cavity.

To evaluate the frequency stability of the obtained regime, using the HCA-S-200M In-GaAs photodetector (FEMTO, Berlin, Germany) and the ESA FSL 3 model.03 RF spectrum analyzer (Rohde&Schwarz GmbH&Co. KG, Munich, Germany), we measured the radio frequency (RF) spectrum presented in Figure 4. The RF spectrum within the fundamental pulse repetition rate, which is  $\sim 8.5$  MHz, was measured with a resolution of 300 Hz, and indicates a signal-to-noise ratio (SNR) of 60 dB with excellent pulse-to-pulse regime stability. The full-range RF spectrum (9 kHz–200 MHz) was measured with a 10 kHz resolution and showed no Q-switch laser operation and the absence of spurious frequency modulations.

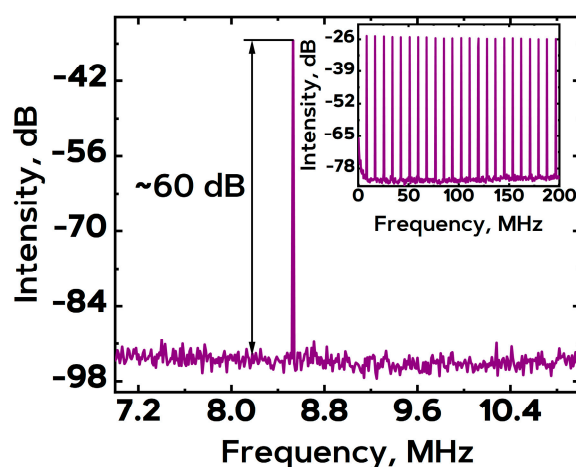


**Figure 4.** RF spectrum of the output pulse train at the fundamental repetition frequency and RF spectrum at the full frequency range (inset).

The output pulse train (obtained with an Infinium MSO9254A oscilloscope (Keysight Technologies, Santa Rosa, CA, USA)) is shown in Figure 5a, inset, and also shows no spurious modulations of the radiation intensity in the obtained regime. To quantify the long-term intensity stability, we measured (with a PM200 power meter (Thorlabs GmbH, Dachau, Germany)) the average output optical power stability for 12 h, and the graph of this measurement is presented in Figure 5a. The standard deviation was  $\sim 1\%$  RMS. This value for mode-locked fiber lasers was mainly due to the lack of thermal stabilization of the system and, as a consequence, the thermal drift of the average output power.

In order to characterize short-term regime stability, we measured the RIN of the USP fiber laser and the noise floor of the receiving system, which includes a photodetector (PD) and an electrical spectrum analyzer (ESA). Figure 5b shows the RIN in the range of 30 Hz–100 kHz (obtained with the ESA SR770FFT (Stanford Research Systems, Sunnyvale, CA, USA) at 250 Hz resolution), where peaks at 30, 59 and 78 kHz may be observed. They are due to external radio-frequency interference. The minimal observed RIN value of the laser is  $< -120$  dBc/Hz. The RIN in the range of 9 kHz–1 MHz (obtained with the ESA FSL 3 model.03 RF spectrum analyzer (Rohde&Schwarz GmbH&Co. KG, Munich, Germany) at 300 Hz resolution) is demonstrated in Figure 5b, inset, and corresponds to a maximum noise level of  $< -102$  dBc/Hz, ensured mainly by the noise floor of the receiving system and signal normalization to the carrier.

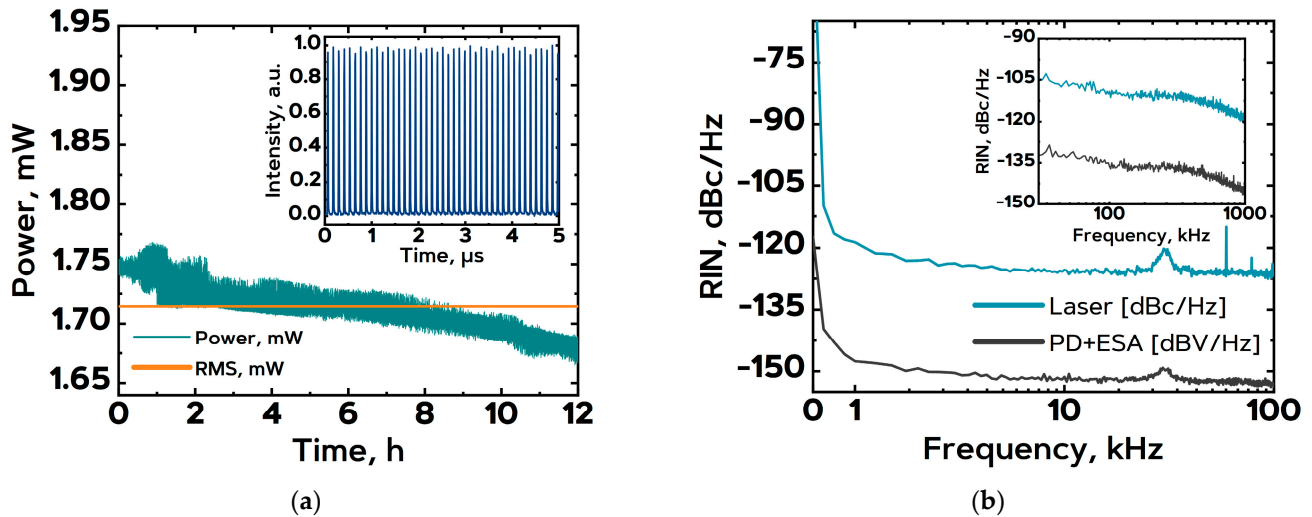


Figure 5. (a) Average output optical power and typical pulse train (inset). (b) RIN of the USP fiber laser and the receiving system noise floor at a low frequency range and RIN at a high frequency range.

To consider the evolution of the pulse, the SMF-28 fiber stretcher–compressor was connected to the output of the laser, then we measured the optical spectrum and the intensity autocorrelation at various fiber lengths and plotted the studied pulse evolution during the propagation of radiation along the fiber using interpolation. The initial fiber length was 22 m, which is slightly greater than the length of the SMF-28 resonator section, and the minimum length of the compressor, due to the features of the measuring circuit, was ~3 m. Figure 6 shows the experimental results for the spectrum evolution, as well as the intensity autocorrelation trace of the obtained regime depending on the length of the fiber compressor length, which, as could be noticed, after passing the extremum point, begins to play the role of a stretcher. The radiation leaves the resonator after 6.09 m EDF with normal dispersion and 1.02 m SMF-28 fiber with anomalous dispersion, and, as a result, it has strong positive chirp, which is compensated by a fiber compressor up to a certain point.

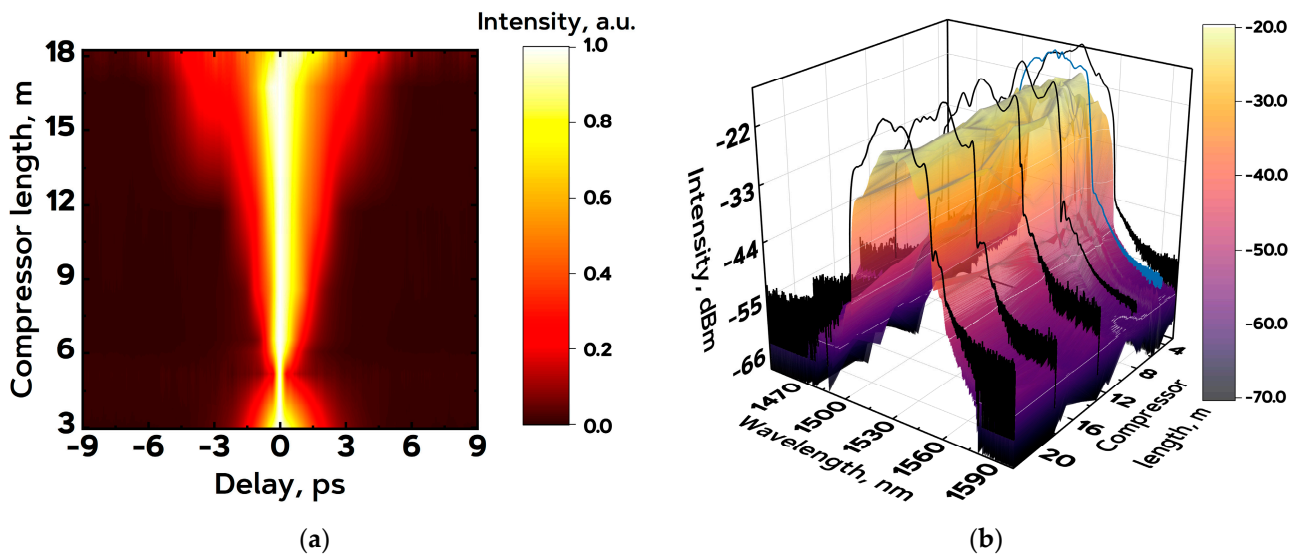


Figure 6. (a) Intensity autocorrelation trace evolution. (b) Optical spectrum evolution.

The evolution of the pulse duration (Figure 6a) is quite even. Distributed in a medium with an anomalous GVD, the pulse is compressed to ~294 fs over a fiber length of ~5.1 m, after which it expands relatively evenly. The evolution of the spectrum (Figure 6b) demon-

states a periodic shift of the emission intensity peak from the central wavelength of 1530 nm to 1540 nm and back. In our opinion, this is due to the effect of the four-wave mixing process. It should also be noted that the generation regime did not change during the experiment.

Figure 7 shows a comparative picture of the evolution of the pulse duration and spectrum width at FWHM. In general, the expansion and narrowing of the spectrum is similar to the compression and stretching in the time domain. However, these two graphs have some discrepancies at certain points. We believe that the reason for this is the process of spectral redistribution of energy caused by the effect of four-wave mixing as the pulse propagates in the output fiber.

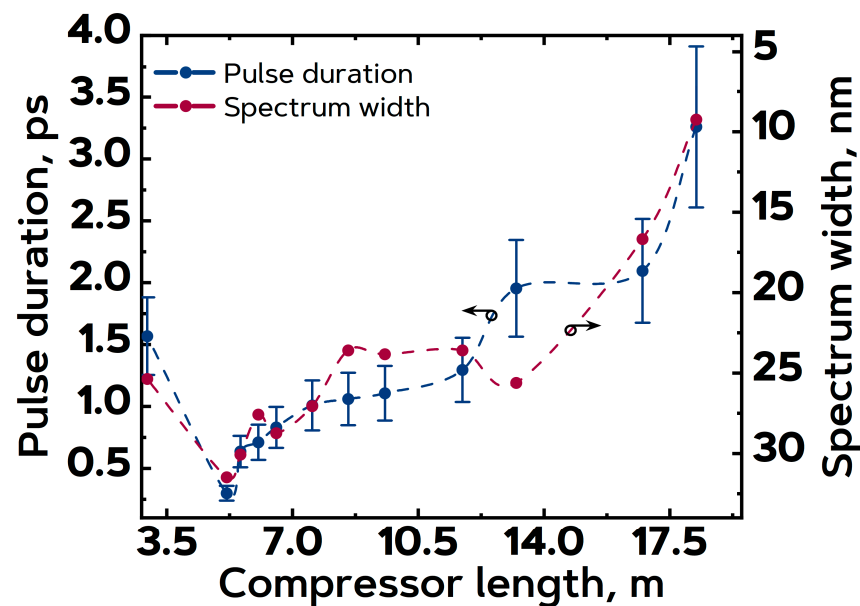


Figure 7. Pulse duration and spectrum width evolution at FWHM depending on compressor length.

According to these results, we can see that the evolution of the spectrum and the pulse duration strongly correlate with each other. The narrowing of the optical spectrum after maximum pulse compression is caused by an imbalance between self-phase modulation (SPM) and anomalous dispersion. The pulse energy at the cavity output is moderate; therefore, when the pulse temporally expands, its low peak power becomes even lower, and self-phase modulation, which determines the number of spectral components of the radiation, decreases. It should also be noted that these graphs characterize the evolution of pulses inside the resonator in the SMF-28 section (between the coupler and the first WDM) with respect to the radiation pulse power. These experimental data were used for verification of a numerical model.

#### 4. Numerical Modeling and Discussion

To obtain deeper insight into the working principle and lasing dynamic, a numerical model based on the modified NLSE solved by the split-step Fourier method was constructed to introduce the propagation of ultrashort pulses in active and passive fibers [38].

$$\frac{\partial A}{\partial z} = -i\frac{\beta_2}{2}\frac{\partial^2 A}{\partial t^2} + i\gamma |A|^2 A + \frac{\hat{g}(\lambda)}{2} A(z, t) - \frac{\alpha}{2} A(z, t), \quad (1)$$

where  $A$  is the slowly varying amplitude of the pulse envelope,  $z$  is the propagation parameter,  $\beta_2$  is the second-order dispersion,  $t$  is the time parameter,  $\gamma$  is the nonlinear parameter,  $\alpha$  is the loss and  $\hat{g}(\lambda)$  is the gain, which is given by the following equation:

$$\hat{g}(\lambda) = \frac{g_0(\lambda)}{\left(1 + \frac{E_0}{E_{sat}}\right)}, \tag{2}$$

where  $g_0(\lambda)$  is the small signal gain and  $E_{sat}$  is the saturation energy of the active fiber, and  $E_0$  was calculated by  $E_0 = \int |A|^2 dt$ . The parameters of the input field and fiber characteristics for numerical simulation are presented in Table 1.

**Table 1.** Parameters of the input field and fiber characteristics for numerical simulation.

Parameter, Unit	SMF-28	CS980	EDF
$\beta_2$ , ps <sup>2</sup> /m	−0.022	0.0028	0.0696
$\gamma$ , 1/W·m	0.001	0.00346	0.00346
$\alpha$ , dB/m	0.00017	0.0002	0.00025
Gain (g), 1/m	0	0	20
Length, m	18.21	2.044	6.09

The output pulses of the simulated system are taken from the coupler with a transmission function  $q = (1 - R_{out} - a)$ , where  $R_{out}$  is the coupling efficiency and  $a$  is the internal loss of the coupler. WDM was considered as a spectral filter with  $\Omega = 30$  nm bandwidth and a Gaussian transmission function in the frequency domain described as follows:

$$K(w) = \exp\left(-\frac{(w - w_0)^2}{2\Omega^2}\right). \tag{3}$$

The effect of the C:BNNTs and NPE were considered as time-domain filters with transmission functions based on the characteristics of SAs. A slow saturable absorber might be described by the following transmission function:

$$\frac{dq_{C:BNNT}}{dt} = -q\left(\frac{1 - \Delta_{C:BNNT}}{\tau}\right) - q\left(\frac{|A|^2}{P_{abs}}\right), \tag{4}$$

where  $\Delta_{C:BNNT}$  is the modulation depth,  $P_{abs}$  is the saturation power and  $\tau$  is the relaxation time of the C:BNNTs. For NPE, we used the following transmission function:

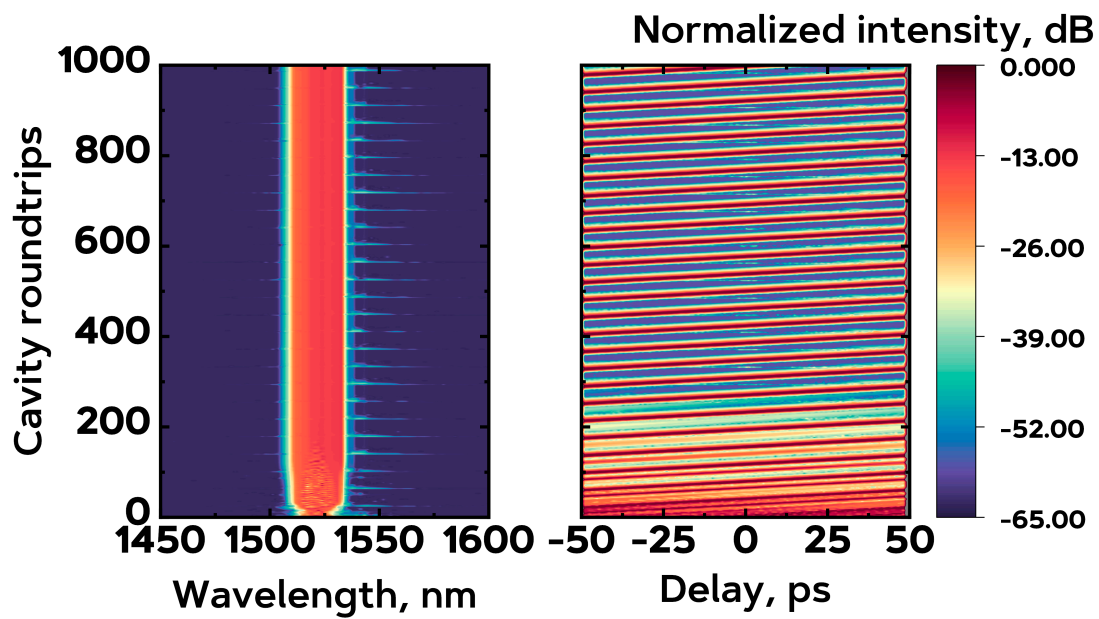
$$q_{NPE} = \frac{\Delta_{NPE}}{1 + \frac{|A|^2}{P_{abs}}}. \tag{5}$$

The parameters of the resonator components specified in the mathematical model are given in Table 2.

Numerical results were recorded after 1000 cavity round trips starting with an input field as a random distribution of energy over the time window. Figure 8 shows the spectral (a) and temporal (b) distributions of the output field intensity, with a time grid equal to 100 ps and a wavelength grid equal to 150 nm. The number of grid points was set as  $2^{13}$ , leading to temporal and spectral resolutions equal to 12 fs and 18 GHz, respectively.

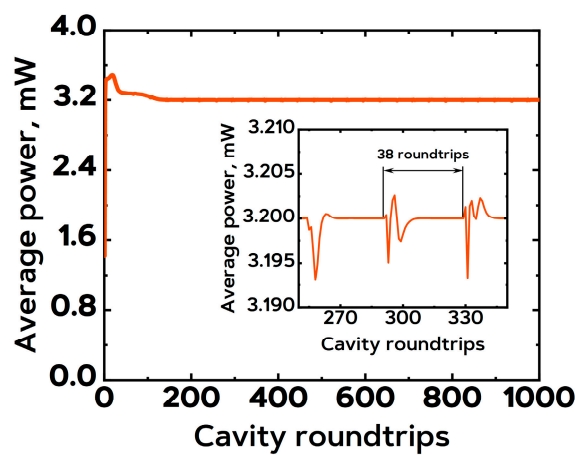
Table 2. Parameters of resonator components.

Element	Parameter	Value
C:BNNTs	Modulation depth	0.3
	Saturation power, W	3
	Recovery time, ps	0.25
Coupler	Coupling ratio	20/80
	Internal loss	0.005
WDM	Filter bandwidth, nm	30
NPE	Saturation power, W	1000
	Modulation depth	0.1



(a)

(b)



(c)

Figure 8. (a) Spectral and temporal (b) distribution of the output field intensity. (c) Evolution of the average output optical power as a function of the position in the cavity and the manifestation of modulation instability (inset).

Looking at the obtained results, one may observe the formation of a two-pulse mode, which evolves into a single-pulse mode and stabilizes after  $\sim 300$  round trips at a center wavelength equal to 1530 nm corresponding to the gain of EDF as an active medium. The

shift of pulse positions within a time window (Figure 8b, x-axis) is determined by the time it takes for the pulse to travel around the resonator, i.e., the length of the cavity. The average output power of the stable pulses (Figure 8c) was calculated by  $P = f_{rep} \int |A(t)|^2 dt$ , and it was equal to 3.2 mW for  $f_{rep} = 8.5$  MHz.

The output peak power in the numerical model is close to the saturation power of C:BNNTs. Therefore, the nanotubes induce modulation instability in the NLSE solution. This instability results in the appearance of wings on the optical spectrum below the  $-40$  dBm level (spikes in Figure 8a) and fluctuations in the output power within 0.2% of the average level (Figure 8c). The period of instability emergence in the simulation results is 38 round trips.

Moreover, in the evolution of the chirp parameter with respect to the propagation length of the laser components, shown in Figure 9a, chirp can be detected by the rate of change in the instantaneous frequency pulse evolution (which essentially represents the temporal derivative of the oscillation phase). The time grid is equal to 60 ps to cover all the changes throughout the simulation process.

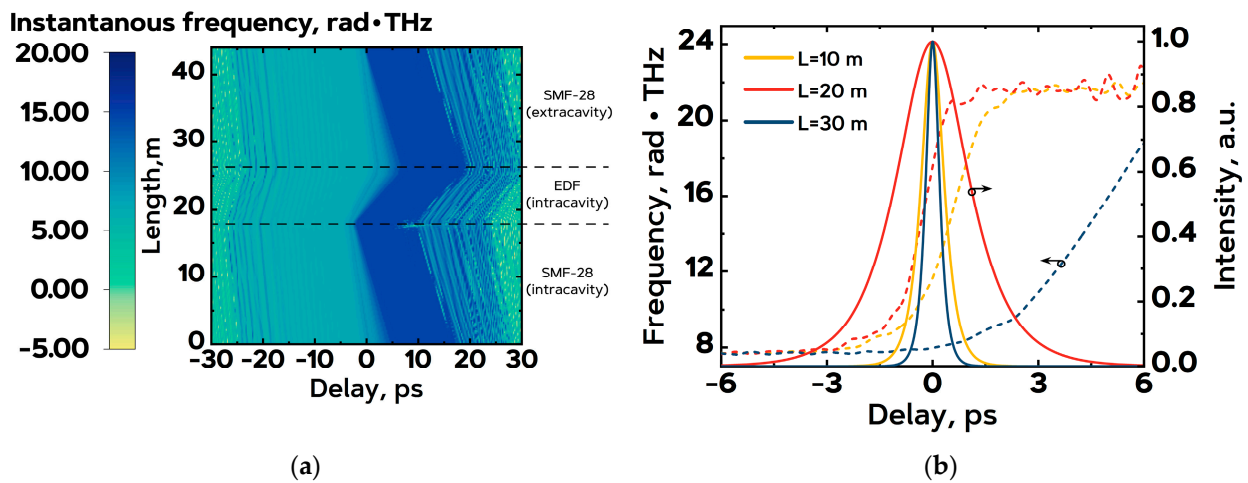


Figure 9. (a) Time-dependent instantaneous frequency as a function of the position in the cavity. (b) The temporal distribution of pulses (solid lines) and time-dependent instantaneous frequency (dotted lines).

This evolution indicates that the pulse leaves the cavity of the resonator with positive sign net chirp. Also, it could be noted that the chirp keeps its positive value along with the propagation in all cavity components, which ensures that the generation regime is a similariton regime [39]. Now, along one round trip of the cavity, chirp has been represented at three points within the propagation length in order to investigate the effect of chirp on the duration of the pulse (Figure 9b). It could be noted that the positive chirp becomes much stronger in the EDF, causing an increase in pulse duration (yellow line in Figure 9b). However, within the propagation in the SMF-28 compressor after the laser cavity, the chirp reaches its minimum value and the rate of change in instantaneous frequency corresponding to the same time domain of the pulse is much less than its value in the cavity (red line in Figure 9b). These results show the ability to compensate for the positive pulse chirp in order to obtain a minimum pulse duration, which was obtained with the minimum positive value of the chirp—in other words, when the instantaneous frequency and the spectral phase of the pulses were nearly equivalent to a constant value.

To obtain complete knowledge of the laser’s operation, the model introduced the evolution of pulse duration and optical power as a function of the position in the laser cavity, as shown in Figure 10. The pulse duration evolution indicates a decrease in  $\tau$  within a propagation in the SMF-28 fiber until it reaches a minimum value (330 fs) before the pulse starts to propagate in highly positive sign chirp fibers. The maximum value of  $\tau \sim 2.24$  ps is at the end of propagation in normal dispersion fibers (under the maximum

value of positive chirp). The pulse compression factor, which is the ratio between the maximum and minimum pulse duration in the cavity, is approximately 7, which ensures the main involvement of the dispersion map and chirp in the pulse shaping mechanism. The demonstrated pulse duration evolution is identical to the similariton pulse duration evolutions in [40,41] and reasonably agrees with the experimental results. The numerical results of the investigation indicate the possibility of using SMF-28 to compress pulses. The SMF-28 fiber outside the cavity compresses the pulse duration from  $\tau = \sim 1.3$  ps at the resonator output to 302 fs at the compressor length of  $\sim 4.6$  m. These results also correlate with what was obtained experimentally. Figure 10b shows the increase in optical power along the propagation in the EDF due to the gain coefficient. Optical losses in all fibers (Table 1) and the optical components were considered. Finally, the optical pulse propagates in the 20% port of the coupler. The final optical power is  $\sim 3.2$  mW.

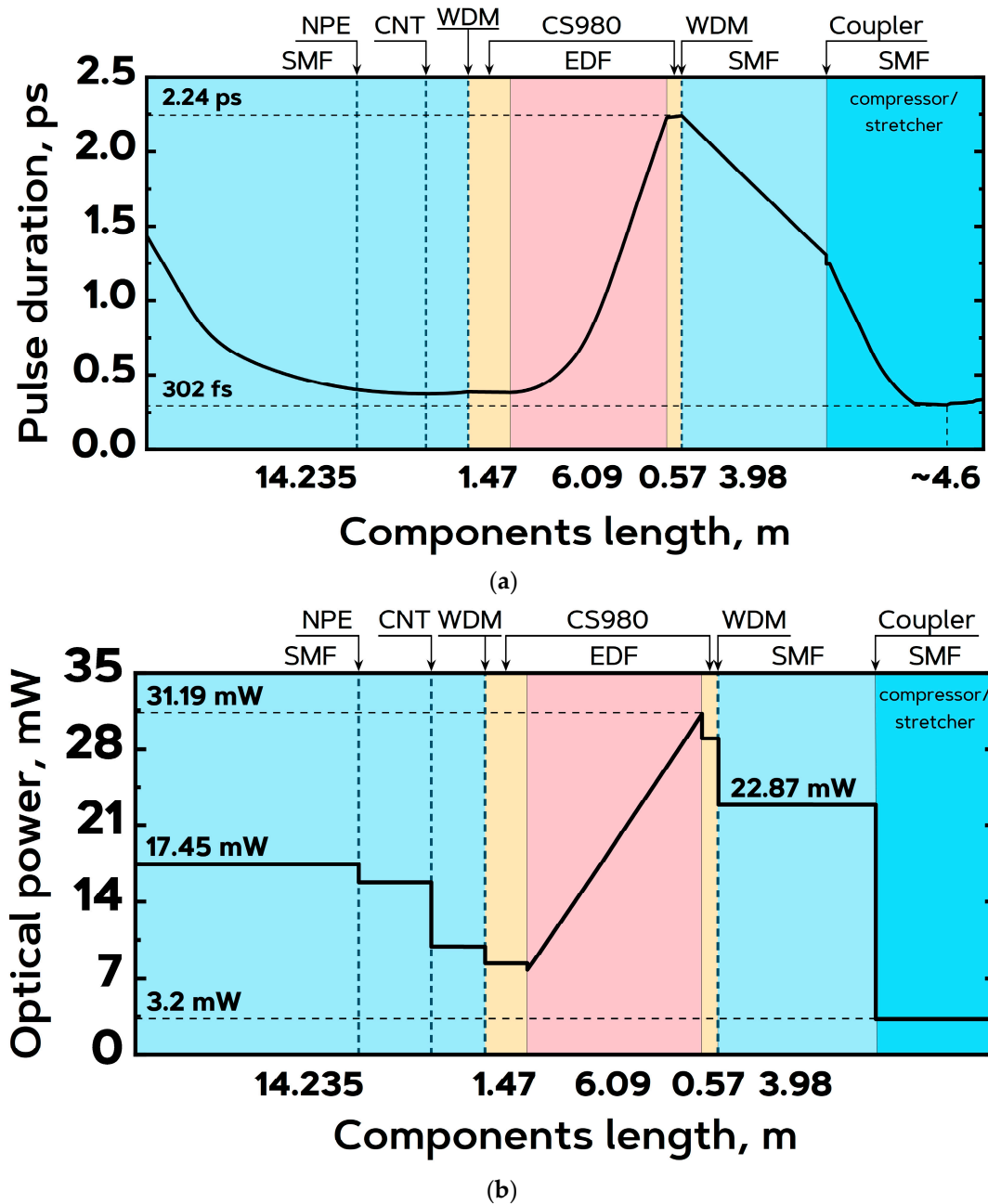


Figure 10. The evolution of pulse duration (a) and the average optical power (b) as a function of the position in the laser cavity.

## 5. Conclusions

In summary, we obtained a similariton regime generated by a 26.5 m long resonator with a normal total net-cavity dispersion of  $\beta_2 = +0.025 \text{ ps}^2$ , with a similariton-like spectrum with an FWHM of 31.5 nm, a pulse duration of  $\sim 294 \text{ fs}$  after compression, and a fundamental repetition rate of 8.5 MHz. The RF spectrum of the radiation corresponds to an SNR of 60 dB at the fundamental repetition frequency. The standard deviation of the average output optical power is about 1% RMS in 12 h of measurement, and the RIN does not exceed  $< -120 \text{ dBc/Hz}$  at the 30 Hz–1 MHz frequency range. For such a regime, we investigated experimentally and numerically the evolution of spectrum and pulse duration in the fiber with anomalous GVD. The dynamics of changes in pulse duration were uniform. We have experimentally shown that a pulse with a duration of  $\sim 1.6 \text{ ps}$  first compressed to  $\sim 294 \text{ fs}$  with an  $\sim 5.1 \text{ m}$  length of fiber and then stretched to  $\sim 3.2 \text{ ps}$ , while according to the numerical simulation, the pulse had an initial duration of  $\sim 1.3 \text{ ps}$  and compressed to 302 fs at a length of 4.6 m. The difference between the numerical and experimental results is in a reasonable range and may be explained by the absence of some factors in the model, such as high-order dispersion parameters with respect to the high peak power pulse propagation in the laser resonator. The evolution of the optical spectrum showed a periodic shift of the intensity maximum from the central wavelength of 1530 nm to the region of 1540 nm because of the effect of four-wave mixing. Pulse dynamics inside the cavity, studied within the model, fully correspond to the regime of similaritons. In this case, the minimum pulse duration inside the resonator is located at the interface between fibers with normal and anomalous dispersion and is 330 fs. Thus, we believe that the study sheds light on the processes of the formation and evolution of similaritons both inside a laser cavity and during propagation in a medium, and we anticipate that this investigation will expand knowledge of the similariton generation mechanisms and provide a clear view of the demonstration and parameter control of USP lasers with normal net-cavity dispersion and a hybrid mode-locking process.

**Author Contributions:** Conceptualization, A.Y.F., D.A.D. and L.K.D.; methodology, A.Y.F., I.O.O., A.I., D.A.D. and V.E.K.; software, A.I. and I.O.O.; validation, S.G.S. and D.A.D.; formal analysis, A.Y.F. and A.I.; investigation, A.Y.F., A.I. and I.O.O.; data curation, A.Y.F., A.I. and I.O.O.; writing—original draft preparation, A.Y.F. and A.I.; writing—review and editing, I.O.O., D.A.D., L.K.D. and V.E.K.; visualization, A.Y.F. and A.I.; supervision, S.G.S.; project administration, S.G.S.; funding acquisition, S.G.S. and V.E.K. All authors have read and agreed to the published version of the manuscript.

**Funding:** This research was funded by the Russian Science Foundation (RSF), grant number 23-19-00700.

**Institutional Review Board Statement:** Not applicable.

**Informed Consent Statement:** Not applicable.

**Data Availability Statement:** The original contributions presented in the study are included in the article; further inquiries can be directed to the corresponding author.

**Conflicts of Interest:** The authors declare no conflicts of interest.

## References

1. Draper, A.D.; Cole, R.K.; Makowiecki, A.S.; Mohr, J.; Zdanowicz, A.; Marchese, A.; Hoghooghi, N.; Rieker, G.B. Broadband Dual-Frequency Comb Spectroscopy in a Rapid Compression Machine. *Opt. Express* **2019**, *27*, 10814. [[CrossRef](#)] [[PubMed](#)]
2. Chang, Z.; Tancin, R.J.; Radhakrishna, V.; Lucht, R.P.; Goldenstein, C.S. Broadband Ultrafast-Laser-Absorption Spectroscopy for Multi-Hydrocarbon Measurements near 3.3 Mm in Flames. *Appl. Opt.* **2023**, *62*, 4681. [[CrossRef](#)] [[PubMed](#)]
3. Ohtsubo, N.; Li, Y.; Nemitz, N.; Hachisu, H.; Matsubara, K.; Ido, T.; Hayasaka, K. Frequency Ratio of an 115 In + Ion Clock and a 87 Sr Optical Lattice Clock. *Opt. Lett.* **2020**, *45*, 5950. [[CrossRef](#)] [[PubMed](#)]
4. Beloy, K.; Bodine, M.I.; Bothwell, T.; Brewer, S.M.; Bromley, S.L.; Chen, J.S.; Deschênes, J.D.; Diddams, S.A.; Fasano, R.J.; Fortier, T.M.; et al. Frequency Ratio Measurements at 18-Digit Accuracy Using an Optical Clock Network. *Nature* **2021**, *591*, 564–569. [[CrossRef](#)]
5. Wang, F.; Xu, E.M.; Dong, J.J.; Zhang, X.L. A Tunable and Switchable Single-Longitudinal-Mode Dual-Wavelength Fiber Laser Incorporating a Reconfigurable Dual-Pass Mach-Zehnder Interferometer and Its Application in Microwave Generation. *Opt. Commun.* **2011**, *284*, 2337–2340. [[CrossRef](#)]

6. Jung, K.; Shin, J.; Kim, J. Ultralow Phase Noise Microwave Generation From Mode-Locked Er-Fiber Lasers With Subfemtosecond Integrated Timing Jitter. *IEEE Photonics J.* **2013**, *5*, 5500906. [[CrossRef](#)]
7. Kalubovilage, M.; Endo, M.; Schibli, T.R. Ultra-Low Phase Noise Microwave Generation with a Free-Running Monolithic Femtosecond Laser. *Opt. Express* **2020**, *28*, 25400. [[CrossRef](#)] [[PubMed](#)]
8. Li, Y.; Cao, X.; Gu, X.; Chen, H.; Zhang, N.; Meng, Y.; Lu, X.; He, L.; Xu, Y.; Wang, F. Sub-Femtosecond Timing Jitter From a SESAM Mode-Locked Yb-Fiber Laser. *IEEE Photonics Technol. Lett.* **2021**, *33*, 1309–1312. [[CrossRef](#)]
9. Cheng, H.; Zhang, Z.; Pan, R.; Zhang, T.; Feng, Y.; Hu, X.; Wang, Y.; Wu, S. Compact, Repetition Rate Locked All-PM Fiber Femtosecond Laser System Based on Low Noise Figure-9 Er:Fiber Laser. *Opt. Laser Technol.* **2023**, *158*, 108818. [[CrossRef](#)]
10. Zhu, Z.; Liu, Y.; Zhang, W.; Luo, D.; Wang, C.; Zhou, L.; Deng, Z.; Li, W. Low-Noise, Robust, All-Polarization-Maintaining Mode-Locked Er-Doped Fiber Ring Laser. *IEEE Photonics Technol. Lett.* **2018**, *30*, 1139–1142. [[CrossRef](#)]
11. Deng, Z.; Liu, Y.; Zhu, Z.; Luo, D.; Gu, C.; Zhou, L.; Xie, G.; Li, W. Ultra-Precise Optical Phase-Locking Approach for Ultralow Noise Frequency Comb Generation. *Opt. Laser Technol.* **2021**, *138*, 106906. [[CrossRef](#)]
12. Benko, C.; Ruehl, A.; Martin, M.J.; Eikema, K.S.E.; Fermann, M.E.; Hartl, I.; Ye, J. Full Phase Stabilization of a Yb:Fiber Femtosecond Frequency Comb via High-Bandwidth Transducers. *Opt. Lett.* **2012**, *37*, 2196. [[CrossRef](#)] [[PubMed](#)]
13. Kim, D.; Zhang, S.; Kwon, D.; Liao, R.; Cui, Y.; Zhang, Z.; Song, Y.; Kim, J. Intensity Noise Suppression in Mode-Locked Fiber Lasers by Double Optical Bandpass Filtering. *Opt. Lett.* **2017**, *42*, 4095. [[CrossRef](#)] [[PubMed](#)]
14. Mayer, A.S.; Grosinger, W.; Fellingner, J.; Winkler, G.; Perner, L.W.; Droste, S.; Salman, S.H.; Li, C.; Heyl, C.M.; Hartl, I.; et al. Flexible All-PM NALM Yb:Fiber Laser Design for Frequency Comb Applications: Operation Regimes and Their Noise Properties. *Opt. Express* **2020**, *28*, 18946. [[CrossRef](#)] [[PubMed](#)]
15. Tamura, K.; Ippen, E.P.; Haus, H.A. Pulse Dynamics in Stretched-Pulse Fiber Lasers. *Appl. Phys. Lett.* **1995**, *67*, 158–160. [[CrossRef](#)]
16. Ilday, F.Ö.; Buckley, J.R.; Clark, W.G.; Wise, F.W. Self-Similar Evolution of Parabolic Pulses in a Laser. *Phys. Rev. Lett.* **2004**, *92*, 213902. [[CrossRef](#)] [[PubMed](#)]
17. Peacock, A.C.; Kruhlak, R.J.; Harvey, J.D.; Dudley, J.M. Solitary Pulse Propagation in High Gain Optical Fiber Amplifiers with Normal Group Velocity Dispersion. *Opt. Commun.* **2002**, *206*, 171–177. [[CrossRef](#)]
18. Wise, F.W.; Chong, A.; Renninger, W.H. High-energy Femtosecond Fiber Lasers Based on Pulse Propagation at Normal Dispersion. *Laser Photon Rev.* **2008**, *2*, 58–73. [[CrossRef](#)]
19. Chen, W.; Song, Y.; Jung, K.; Hu, M.; Wang, C.; Kim, J. Few-Femtosecond Timing Jitter from a Picosecond All-Polarization-Maintaining Yb-Fiber Laser. *Opt. Express* **2016**, *24*, 1347. [[CrossRef](#)]
20. Ouyang, C.; Shum, P.; Wang, H.; Haur Wong, J.; Wu, K.; Fu, S.; Li, R.; Kelleher, E.J.R.; Chernov, A.I.; Obraztsova, E.D. Observation of Timing Jitter Reduction Induced by Spectral Filtering in a Fiber Laser Mode Locked with a Carbon Nanotube-Based Saturable Absorber. *Opt. Lett.* **2010**, *35*, 2320. [[CrossRef](#)]
21. Yu, Z.; Ou, S.; Guo, L.; Zhang, Q.; Sui, Q.; Chen, Y.; Zhang, N.; Liu, H.; Shum, P.P. 109 Fs, 553 MHz Pulses from a Polarization-Maintaining Yb-Doped Ring Fiber Laser with SESAM Mode-Locking. *Opt. Commun.* **2022**, *522*, 128520. [[CrossRef](#)]
22. Huang, L.; Zhang, Y.; Liu, X. Dynamics of Carbon Nanotube-Based Mode-Locking Fiber Lasers. *Nanophotonics* **2020**, *9*, 2731–2761. [[CrossRef](#)]
23. Cheng, C.-H.; Lin, G.-R. Carbon Nanomaterials Based Saturable Absorbers for Ultrafast Passive Mode-Locking of Fiber Lasers. *Curr. Nanosci.* **2020**, *16*, 441–457. [[CrossRef](#)]
24. Dvoretzkiy, D.A.; Sazonkin, S.G.; Orekhov, I.O.; Kudelin, I.S.; Pnev, A.B.; Karasik, V.E.; Krylov, A.A.; Denisov, L.K. High-Energy Ultrashort-Pulse All-Fiber Erbium-Doped Ring Laser with Improved Free-Running Performance. *J. Opt. Soc. Am. B* **2018**, *35*, 2010. [[CrossRef](#)]
25. Yu, Y.; Teng, H.; Wang, H.; Wang, L.; Zhu, J.; Fang, S.; Chang, G.; Wang, J.; Wei, Z. Highly-Stable Mode-Locked PM Yb-Fiber Laser with 10 NJ in 93-Fs at 6 MHz Using NALM. *Opt. Express* **2018**, *26*, 10428. [[CrossRef](#)] [[PubMed](#)]
26. Wang, M.; Liu, M.; Chen, Y.; Ouyang, D.; Zhao, J.; Pei, J.; Ruan, S. Stable Noise-like Pulse Generation in All-PM Mode-Locked Tm-Doped Fiber Laser Based on NOLM. *Chin. Opt. Lett.* **2021**, *19*, 091402. [[CrossRef](#)]
27. Chernysheva, M.A.; Krylov, A.A.; Mou, C.; Arif, R.N.; Rozhin, A.G.; Rummelli, M.H.; Turitsyn, S.K.; Dianov, E.M. Higher-Order Soliton Generation in Hybrid Mode-Locked Thulium-Doped Fiber Ring Laser. *IEEE J. Sel. Top. Quantum Electron.* **2014**, *20*, 425–432. [[CrossRef](#)]
28. Chernykh, D.S.; Krylov, A.A.; Levchenko, A.E.; Grebenyukov, V.V.; Arutunyan, N.R.; Pozharov, A.S.; Obraztsova, E.D.; Dianov, E.M. Hybrid Mode-Locked Erbium-Doped All-Fiber Soliton Laser with a Distributed Polarizer. *Appl. Opt.* **2014**, *53*, 6654. [[CrossRef](#)] [[PubMed](#)]
29. Dvoretzkiy, D.A.; Sazonkin, S.G.; Orekhov, I.O.; Kudelin, I.S.; Denisov, L.K.; Karasik, V.E.; Agafonov, V.N.; Khabashesku, V.N.; Davydov, V.A. Femtosecond Er-Doped All-Fiber Laser with High-Density Well-Aligned Carbon-Nanotube-Based Thin-Film Saturable Absorber. *Nanomaterials* **2022**, *12*, 3864. [[CrossRef](#)]
30. Du, Y.; Shu, X. Transformation From Conventional Dissipative Solitons to Amplifier Similaritons in All-Normal Dispersion Mode-Locked Fiber Lasers. *IEEE Photonics J.* **2018**, *10*, 1500911. [[CrossRef](#)]
31. Lapre, C.; Billet, C.; Meng, F.; Ryczkowski, P.; Sylvestre, T.; Finot, C.; Genty, G.; Dudley, J.M. Real-Time Characterization of Spectral Instabilities in a Mode-Locked Fibre Laser Exhibiting Soliton-Similariton Dynamics. *Sci. Rep.* **2019**, *9*, 13950. [[CrossRef](#)] [[PubMed](#)]

32. Boscolo, S.; Turitsyn, S.K.; Finot, C. Amplifier Similariton Fiber Laser with Nonlinear Spectral Compression. *Opt. Lett.* **2012**, *37*, 4531. [[CrossRef](#)] [[PubMed](#)]
33. Chong, A.; Renninger, W.H.; Wise, F.W. Properties of Normal-Dispersion Femtosecond Fiber Lasers. *J. Opt. Soc. Am. B* **2008**, *25*, 140. [[CrossRef](#)]
34. Luo, Y.; Xiang, Y.; Xia, R.; Ni, W.; Liu, B.; Shum, P.P.; Tang, X.; Liu, D.; Sun, Q. Breathing Dynamics in a Gain-Guided Dissipative Soliton-Similariton Fiber Laser. *IEEE Photonics Technol. Lett.* **2020**, *32*, 481–484. [[CrossRef](#)]
35. Zhao, L.M.; Lu, C.; Tam, H.Y.; Wai, P.K.A.; Tang, D.Y. High Fundamental Repetition Rate Fiber Lasers Operated in Strong Normal Dispersion Regime. *IEEE Photonics Technol. Lett.* **2009**, *21*, 724–726. [[CrossRef](#)]
36. Krylov, A.A.; Sazonkin, S.G.; Arutyunyan, N.R.; Grebenyukov, V.V.; Pozharov, A.S.; Dvoretzkiy, D.A.; Obraztsova, E.D.; Dianov, E.M. Performance Peculiarities of Carbon-Nanotube-Based Thin-Film Saturable Absorbers for Erbium Fiber Laser Mode-Locking. *J. Opt. Soc. Am. B* **2016**, *33*, 134. [[CrossRef](#)]
37. Wang, Z.; Zhan, L.; Fang, X.; Gao, C.; Qian, K. Generation of Sub-60 Fs Similaritons at 1.6 Mm From an All-Fiber Er-Doped Laser. *J. Light. Technol.* **2016**, *34*, 4128–4134. [[CrossRef](#)]
38. Agrawal, G.P. Pulse Propagation in Fibers. In *Nonlinear Fiber Optics*; Elsevier: Amsterdam, The Netherlands, 2019; pp. 27–55.
39. Sazonkin, S.G.; Orekhov, I.O.; Dvoretzkiy, D.A.; Lazdovskaia, U.S.; Ismael, A.; Denisov, L.K.; Karasik, V.E. Analysis of the Passive Stabilization Methods of Optical Frequency Comb in Ultrashort-Pulse Erbium-Doped Fiber Lasers. *Fibers* **2022**, *10*, 88. [[CrossRef](#)]
40. Liu, H.; Liu, Z.; Lamb, E.S.; Wise, F. Self-Similar Erbium-Doped Fiber Laser with Large Normal Dispersion. *Opt. Lett.* **2014**, *39*, 1019. [[CrossRef](#)]
41. Oktem, B.; Ülgüdür, C.; Ilday, F.Ö. Soliton-Similariton Fibre Laser. *Nat. Photonics* **2010**, *4*, 307–311. [[CrossRef](#)]

**Disclaimer/Publisher’s Note:** The statements, opinions and data contained in all publications are solely those of the individual author(s) and contributor(s) and not of MDPI and/or the editor(s). MDPI and/or the editor(s) disclaim responsibility for any injury to people or property resulting from any ideas, methods, instructions or products referred to in the content.